Institut de Physique Nucléaire de Lyon

Université Claude Bernard

IN2P3 - CNRS

LYCEN 9617
Juillet 1996

Dipole bands and multi-particle excitations in ^{193}Pb.

L. Ducroux [1], A. Astier[1], R. Duffait[1], Y. Le Coz[1,2], M. Meyer[1], S. Perries[1], N. Redon[1], J.F. Sharpey-Schafer[3,4], A.N. Wilson[3], R. Lucas[2], V. Meot[2], R. Collatz[5], I. Deloncle[5], F. Hannachi[5], A. Lopez-Martens[5], M.G. Porquet[5], C. Schück[5], F. Azaiez[6], S. Bouneau[6], C. Bourgeois[6], A. Korichi[6], N. Poffé[6,7], H. Sergolle[6], B.J.P. Gall[8], I. Hibbert[9] and R. Wadsworth[9]

[1]*IPN Lyon IN2P3/CNRS, Université Claude Bernard,*
F-69622 Villeurbanne Cedex, France
[2]*DAPNIA/SPhN, CE Saclay, 91191 Gif-sur-Yvette Cedex, France*
[3]*Univ. of Liverpool, Liverpool L69 3BX, United Kingdom*
[4]*NAC, Faure, ZA-7131 South Africa*
[5]*CSNSM, IN2P3/CNRS, F-91405 Orsay Campus, France*
[6]*IPN,IN2P3/CNRS, F-91406 Orsay Campus, France*
[7]*Univ. of Oxford, Oxford OX1 3RH, United Kingdom*
[8]*CRN Strasbourg, IN2P3/CNRS, F-67037 Strasbourg Cedex 2, France*
[9]*Univ. of York, York YO1 5DD, United Kingdom*

To be published in Z. Phys. A.

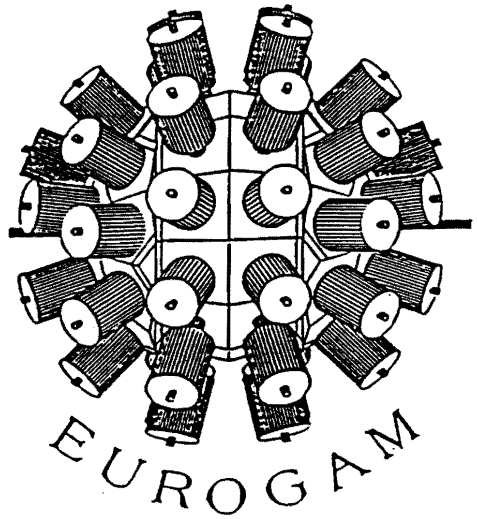

FRANCE - UK
Collaboration

Dipole bands and multi-quasiparticle excitations in ^{193}Pb

L. Ducroux, A. Astier, R. Duffait, Y. Le Coz*, M. Meyer, S. Perries, N. Redon
Institut de Physique Nucléaire de Lyon, IN2P3/CNRS,
Université C. Bernard Lyon-1, F-69622 Villeurbanne Cedex, France
J.F. Sharpey-Schafer†, A.N. Wilson
Oliver Lodge Laboratory, University of Liverpool,
PO Box 147, Liverpool L69 3BX, United Kingdom
R. Lucas, V. Méot
DAPNIA/SPhN, CEA Saclay, 91191 Gif-sur-Yvette Cedex, France
R. Collatz, I. Deloncle, F. Hannachi, A. Lopez-Martens, M.G. Porquet, C. Schück
Centre de Spectrométrie Nucléaire et de Spectroscopie de Masse, IN2P3/CNRS,
Bât. 104, F-91405 Orsay Campus, France
F. Azaiez, S. Bouneau, C. Bourgeois, A. Korichi, N. Poffé‡ , H. Sergolle
Institut de Physique Nucléaire, IN2P3/CNRS,
Bât. 104, F-91406 Orsay Campus, France
B.J.P. Gall
Centre de Recherches Nucléaires de Strasbourg, IN2P3/CNRS,
BP 28, F-67037 Strasbourg Cedex 2, France
I. Hibbert, R. Wadsworth
Department of Physics, University of York,
Heslington, York YO1 5DD, United Kingdom

Abstract : The nucleus ^{193}Pb was populated via the ^{168}Er(^{30}Si,5n) reaction at a beam energy of 159 MeV and studied with the EUROGAM II spectrometer. Five new dipole $\Delta I = 1$ cascades have been found. These structures have been connected to the level scheme which has been considerably extended up to a spin of $\frac{61}{2}$ $\hbar$ and an excitation energy of about 8 MeV. Angular distribution coefficients, a_2, have been measured and confirm the dipole character of the in-band transitions. B(M1)/B(E2) ratios have been extracted for the two most intense cascades. The ^{193}Pb dipole bands are discussed in comparison with those known in odd lead isotopic series and the structure of the band heads is analyzed in terms of microscopic HF+BCS calculations. The proposed configurations are based on a high-K two quasiproton excitation, $\pi\left([505]9/2^- \otimes [606]13/2^+\right)_{K=11^-}$, coupled to one or three rotation aligned quasineutrons involving the $i_{13/2}$, $p_{3/2}$, $f_{5/2}$ and/or $h_{9/2}$ subshells. The main difference, compared with the heavier lead isotopes, is the presence of large Ω orbitals from the $\nu\left(i_{13/2}\right)$ shell near the Fermi surface which are responsible for the increasing band-head spin as A decreases.

PACS : 21.10.Hw, 23.20.Lv, 27.80.+w

---

* *present address : DAPNIA/SPhN, CEA Saclay, 91191 Gif-sur-Yvette Cedex, France*
† *present address: National Accelerator Centre, PO Box 72, Faure, ZA-7131 South Africa*
‡ *present address : Department of Physics, University of Oxford, Keble Road, Oxford OX1 3RH, United Kingdom*

I. Introduction

The A=190 mass region has been widely investigated since the discovery of a superdeformed (SD) band in ^{191}Hg [1]. Recently six SD bands have been discovered and discussed in ^{193}Pb [2,3]. This nucleus is the lightest odd lead isotope where superdeformation has been found. Thanks to the interest devoted to this mass region a new phenomenon was identified with the observation of dipole cascades in heavier lead nuclei $^{198-200}$Pb [4,5]. Many similar bands are now known to exist in lighter lead isotopes [6-20]. In a few cases lifetime measurements have been performed [17,21-24] showing a low quadrupole collectivity and small deformation. These dipole bands have similar properties : most of them are regular (i.e. they show a smooth increase of transition energy with spin) with low dynamical moments of inertia $J^{(2)}$ (15-25 $\hbar^2 MeV^{-1}$) and large B(M1)/B(E2) ratios (>10 $(\mu_N/eb)^2$). In most cases the bands are connected to the low-lying level scheme enabling both spins and excitation energies to be determined. These structures are interpreted as high-K weakly deformed oblate states, built on high-j quasiprotons, coupled to rotation aligned quasineutrons.

An interesting question is whether these structures can be observed in very light lead nuclei such as ^{193}Pb. This nucleus has been previously studied by Lagrange et al. [25] using the reaction ^{182}W(^{16}O,5n) at a 109 MeV beam energy. The low-lying yrast levels and transitions have been extensively investigated by both $e^-\gamma$ and $\gamma\gamma$ coincidence techniques. In this paper we present results on ^{193}Pb obtained in a study with the EUROGAM II spectrometer [26]. The level scheme has been considerably extended and the multipolarity of most of the transitions determined by angular distribution measurements. Five new $\Delta I = 1$ structures have been observed and connected to the low-lying states. The five new dipole $\Delta I = 1$ bands in ^{193}Pb and the evolution of these structures in the isotopic series from A=192 to 200, are discussed in terms of static mean field Hartree-Fock+BCS calculations [27-28]. These bands are interpreted as high-K two quasiproton excitations, $\pi\left([505]9/2^- \otimes [606]13/2^+\right)_{K=11^-}$, coupled to rotation aligned quasineutrons, $\nu\left(i_{13/2}\right)^n$ (with n=1,3) and $\nu\left(\left(i_{13/2}\right)^2 \otimes \left(p_{3/2} \text{ or } f_{5/2}\right)\right)$ and/or $\nu\left(\left(i_{13/2}\right) \otimes \left(h_{9/2}\right)^2\right)$ involving the large Ω orbitals of $\nu\left(i_{13/2}\right)$ ($\Omega = 5/2,\ 7/2$). The departure from the strong coupling model in terms of tilted-axis cranking model [29] is also considered.

II. Experiment and results

Excited states in ^{193}Pb were populated using the ^{168}Er(^{30}Si,5n) reaction. The Si beam at 159 MeV energy was delivered by the Vivitron accelerator at the Centre de Recherches Nucléaires in Strasbourg. The measurement was made with a stack of two self-supporting thin 600 $\mu g/cm^2$ targets. The γ-rays were detected in the EUROGAM II spectrometer [26] which consists of 15 large escape suppressed Ge detectors at backward and forward angles respectively, and 24 escape suppressed "clover" Ge detectors near 90° relative to the beam direction.

A total of 6×10^8 four- and higher fold events were recorded on magnetic tapes, about 40% of the events corresponding to ^{193}Pb residues. The other main open channels were : ^{192}Pb (~20% of the events), ^{190}Hg (~15%) and ^{193}Tl (~12%). The data analysis has been performed by means of multigated spectra and two-dimensional matrices. Moreover a $\gamma\gamma\gamma$ cube has also been built and analysed using the analysis package LEVIT8R [30]. Angular distributions have been measured using four matrices corresponding to the four independent angles of EUROGAM II (22°, 46°, 71° and 80°). Each matrix contains γ-rays detected at one angle on the first axis in coincidence with transitions at any angle on the second axis. Furthermore the matrices were gated on several yrast transitions in the level scheme in order to select the ^{193}Pb nucleus.

The level scheme, previously established up to spin 33/2 $\hbar$ and 3.2 MeV excitation energy by Lagrange et al. [25], has been both significantly extended (up to 7932 keV and spin 61/2 $\hbar$) and modified at lower excitation energy. For instance previous work had not observed the 311 keV transition ($27/2^+ \rightarrow 25/2^+$) and all group B (see below for the label explanation) representing about 50% of the 2213 keV ($25/2^+$) level feeding intensity. Furthermore the cascade built on the 1994 keV ($25/2^+$) state and beginning with the 677 keV transition was not observed in the previous work. More than one hundred fifty γ-rays have been included in the new level scheme shown in Figure 1. Table 1 contains the energies and intensities (normalized at 100% for the $17/2^+ \rightarrow 13/2^+$ 881.6 keV transition) for all the transitions. For the most intense γ-rays the angular coefficient a_2 has been extracted and the results are in excellent agreement with those of Lagrange et al. [25] obtained by electron measurements, with the exception of two transitions, 180 and 556 keV, located above the 22 ns isomeric state at 1586 keV. The explanation for the different assignments of the 556 keV multipolarity is probably due to the presence of another transition of 555 keV ($29/2^+ \rightarrow 27/2^+$, Group B in Fig. 1), twice as intense and of $\Delta I = 1$ nature. This transition was unresolved in the previous experiment. Concerning the 180 keV transition case, our angular distribution measurement clearly suggests a $\Delta I = 1$ multipolarity as opposed to the $\Delta I = 2$ one previously assigned with extremely low statistics.

It is convenient to give labels to different groups in the level scheme in Figure 1. Thanks to the similarity of the low-lying states of ^{193}Pb and those of ^{195}Pb we will adopt the label ordering chosen by M. Kaci et al. [20]. Group A is built on the $13/2^+$ state which is suggested by Lagrange et al. [25] to be nearly 100 keV above the $p_{3/2}$ ground state. Because of the lack of an experimental measurement of this value we will consider the $13/2^+$ level as the reference for excitation energies. Group B is built on top of group A and contains intense dipole $\Delta I = 1$ (M1) and cross-over $\Delta I = 2$ (E2) transitions deexciting positive parity states. A sequence of five $\Delta I = 1$ and four $\Delta I = 2$ transitions seems to appear in this complex group B, starting at the 2426 keV ($27/2^+$) level and extending to the 4313 keV ($37/2^+$) level. In this range of excitation energy, the intensity of this

structure is weaker than the other ones, for instance, the one based in the 2524 keV level. An ensemble of mainly quadrupole transitions can be gathered into group C. These are built on the 22 ns isomeric state ($21/2^-$ at 1586 keV). Finally group D comprises all levels above the 11 ns isomeric state at 2584 keV ($29/2^-$).

In the present work five new $\Delta I = 1$ structures have been clearly identified and the dipole nature of their transitions unambiguously demonstrated by angular distribution measurements. Intensity arguments require a magnetic character of these $\Delta I = 1$ transitions. All these dipole bands have a rotational behaviour with regularly spaced transitions. The exceptions to this are tops of bands 1 and 2 where one can observe (see Figure 1) backbending indicating pair breaking. All these dipole bands have been connected to the low-lying level scheme enabling their excitation energies and spin values to be determined. The five dipole bands can be separated into two sets with opposite parity. Bands 1, 1a, 1b have negative parity and bands 2, 3 positive parity. For bands 1, 2, 3 the labels have been taken to be the same as similar bands in heavier Pb isotopes with respect to intensity criteria. For the weakest bands 1a and 1b the labels recall the fact that they are built on band 1.

Band 1 is the most intense of the five bands with about 17% of the total intensity of the reaction channel. Starting at 2584 keV on the $29/2^-$ isomeric state (11 ns), band 1 extends up to 5218 keV ($45/2^-$) and decays to group A levels.

Both bands 1a and 1b (each $\sim 0.6\%$ intensity) are built on the top of band 1. Band 1a starts at 5092 keV at spin $45/2^-$ and is observed up to the 7154 keV level ($57/2^-$). Band 1b displays a regular behaviour at slightly higher excitation energy (5825 keV) and spin ($49/2^-$) than band 1a, and extends up to 7713 keV ($61/2^-$).

On the positive parity side we have found two regular bands decaying to group B, labelled 2 and 3, with intensities of $\sim 7\%$ and 3% respectively. Band 2 is located at 4297 keV ($39/2^+$) up to 7932 keV ($61/2^+$) and band 3 is built on the 4944 keV level ($43/2^+$) reaching 6145 keV ($51/2^+$).

Triple gated spectra showing the five dipole $\Delta I = 1$ bands are displayed in Figure 2 (for bands 1, 1a and 1b) and Figure 3 (for bands 2 and 3).

For the two most intense bands (1 and 2) E2 cross-over transitions can be observed allowing us to extract the experimental transition probability ratios B(M1)/B(E2) with the hypothesis that $\Delta I = 1$ transitions have a pure magnetic character. The B(M1)/B(E2) ratios are summarized in Table 2.

III. Discussion

A large number of dipole $\Delta I = 1$ bands are known in lead isotopes [4-24]. These structures have been interpreted in terms of weakly oblate-deformed high-K quasiprotons $\pi([505]9/2^- \otimes [606]13/2^+)_{K=11^-}$ and $\pi([505]9/2^- \otimes [514]7/2^-)_{K=8^+}$ coupled to rotation

aligned quasineutrons from $i_{13/2}$, $f_{5/2}$ and $p_{3/2}$ orbitals. For the following we will use the notation of the cranked shell model introduced by H. Hübel et al. [31] in ^{194}Hg (A, B, C and D for $i_{13/2}$, E and F for $f_{5/2}$ and $p_{3/2}$ orbitals) but in order to discuss the properties of the isotopic lead series from A=192 to A=200 we will also use the complete orbital labels. As we discuss below, comparison of the dipole bands of ^{193}Pb with those in the heavier lead isotopes, ^{195,197,199}Pb [20,18,15], allows the following configuration assignments to be suggested :

$$\nu\left(i_{13/2}\right) \otimes \pi\left([505]9/2^- \otimes [606]13/2^+\right)_{K=11^-} \text{, called A11 (band 1)}$$

$$\nu\left(i_{13/2}\right)^3 \otimes \pi\left([505]9/2^- \otimes [606]13/2^+\right)_{K=11^-} \text{, called ABC11 (band 1a)}$$

$$\left.\begin{array}{l} \nu\left(\left(i_{13/2}\right)^2 \otimes \left(p_{3/2}\right)\right) \otimes \pi\left([505]9/2^- \otimes [606]13/2^+\right)_{K=11^-} \\ \nu\left(\left(i_{13/2}\right)^2 \otimes \left(f_{5/2}\right)\right) \otimes \pi\left([505]9/2^- \otimes [606]13/2^+\right)_{K=11^-} \end{array}\right\} \text{called ABE/F11 (bands 2,3)}$$

Concerning the structure in group B discussed above, the lowest state lies at the same range of excitation energy than the 11 ns isomeric state $(29/2^-)$ at 2584 keV. Its configuration should be of three quasiparticule excitation type. A possible interpretation could be :

$$\nu\left(i_{13/2}\right) \otimes \pi\left([505]9/2^- \otimes [514]7/2^-\right)_{K=8^+} \text{, called A8}$$

not definitively observed, up to now, in heavier lead isotopes. At this point of the discussion the spin values of the band heads are not understood and the configuration assignment of the last new dipole $\Delta I = 1$ band (1b) remains unknown.

Band 1 is built on the $29/2^-$ isomeric state (11 ns) at 2584 keV and consists of 8 $\Delta I = 1$ transitions up to the spin $45/2^-$. The spin and parity of the band head lead us to propose the three quasiparticle $\nu\left(i_{13/2}\right) \otimes \pi\left([505]9/2^- \otimes [606]13/2^+\right)_{K=11^-}$ configuration (called A11) for this band. This is corroborated by the following points :

i) For all dipole bands observed in odd (even) Pb isotopes, the K=11^- two quasiproton excitation, coupled to a one quasineutron (two quasineutron respectively) excitation, is the most intense. This is also the case for band 1 in ^{193}Pb. Moreover the excitation energy of the band head fits perfectly with the systematics of the similar configuration A11 observed in ^{195,197,199}Pb [20,18,15] presented in Figure 4.

ii) The energy of the A11 configuration can be roughly estimated using the experimental energies of the K=11^- quasiproton states of neighbouring even ^{192,194}Pb isotopes [13,14] and the $\nu\left(i_{13/2}\right)$ energy in ^{193}Pb :

$$E(A11,^{193}\,\mathrm{Pb}) \simeq \frac{1}{2}\left[E(11^-,^{192}\,\mathrm{Pb}) + E(11^-,^{194}\,\mathrm{Pb})\right] + E(13/2^+,^{193}\,\mathrm{Pb})$$

$$\simeq 2838 \text{ keV}$$

This value is in reasonable agreement with the experimental energy of 2584 keV observed for the A11 band head.

iii) The mean value of the extracted B(M1)/B(E2) ratio is 22±7 $(\mu_N/eb)^2$, in the same range that the experimental B(M1)/B(E2) ratios of the similar bands in ^{195,197,199}Pb [20,23,24]. This large value of the B(M1)/B(E2) ratio (> 10 $(\mu_N/eb)^2$), typical for lead isotopes, implies a strong B(M1) and then a high-K configuration.

Above band 1 two sub-structures are observed, labelled 1a and 1b, decaying to band 1. One can clearly consider band 1a as based on a five quasiparticle excitation and more precisely on a two quasineutron excitation added to the A11 configuration, occuring at the spin of $45/2^-$ and at the excitation energy of 5092 keV. This is corroborated by two facts :

i) Figure 5a compares the behaviour of the angular momentum projections I_x along the rotational axis as a function of the rotational frequency for bands 1-1a in ^{193}Pb to those reported in ^{195,197,199}Pb [20,18,15] and interpreted as A11 at low spin and ABC11 (i.e. $\nu\left(i_{13/2}\right)^3 \otimes \pi\left([505]9/2^- \otimes [606]13/2^+\right)_{K=11^-}$) at high spin. The progressive alignment of an $i_{13/2}$ neutron pair along the rotational axis occurs at the same frequency of about 0.35 MeV for all these four odd Pb isotopes. The systematics exhibit another similar characteristic, the gain in terms of I_x of about 10 $\hbar$ at the frequency of 0.3 MeV.

ii) We can estimate the ABC11 experimental excitation energy from both K=11^- level in ^{192,194}Pb and yrast $33/2^+$ state (ABC) in ^{193}Pb :

$$E(ABC11,^{193}\,\mathrm{Pb}) \simeq \frac{1}{2}\left[E(11^-,^{192}\,\mathrm{Pb}) + E(11^-,^{194}\,\mathrm{Pb})\right] + E(33/2^+,^{193}\,\mathrm{Pb})$$
$$\simeq 5451 \text{ keV}$$

This value is close to the 5091 keV experimental value for the band head of band 1a. Therefore this leads us to propose the configuration ABC11 for band 1a.

Concerning band 1b, it is worth noting that such a dipole band has never been observed in heavier Pb isotopes. It appears weakly at higher excitation energy (5825 keV) and spin $(49/2^-)$ than band 1a. Band 1b is well established in the level scheme and connected to band 1 via three dipole transitions 354, 320 and 323 keV which we assume are M1. Thus, band 1b has the same negative parity as band 1 (and 1a). The interpretation of this band will be discussed in more detail later.

Bands 2 and 3 can be discussed together. They occur at 4296 keV and 4944 keV excitation energy respectively, and are built on the positive states $39/2^+$ and $43/2^+$ respectively. Three alternative configurations can be proposed satisfying spin and parity for the two band heads : $\nu\left(i_{13/2}\right)^3 \otimes \pi\left([505]9/2^- \otimes [514]7/2^-\right)_{K=8^+}$ (i.e. ABC8) and $\nu\left(\left(i_{13/2}\right)^2 \otimes \left(p_{3/2} \text{ or } f_{5/2}\right)\right) \otimes \pi\left([505]9/2^- \otimes [606]13/2^+\right)_{K=11^-}$ (i.e. ABE/F11). In ^{197,199}Pb [18,15] both ABE11 and ABF11 have been observed and the most intense band has been labelled ABE11. The following considerations lead us to propose these two latter configurations to understand these two bands.

i) The systematics in terms of projection of the angular momentum on the rotational axis and of excitation energy confirm this ABE/F11 assignment (see Figures 5b, 5c). In

particular it is worth noting that the alignment of an $i_{13/2}$ neutron pair occurs at the top of band 2 in ^{193}Pb as was the case for the same band in ^{195,197}Pb [20,18].

ii) The behaviour of the moment of inertia is quite similar to that of band c in ^{194}Pb [12] interpreted as AB11 at low spin and ABCD11 at high spin. The saturation due to the alignment of the next $i_{13/2}$ neutron pair (CD), observed in both cases in Figure 6, appears at the same frequency (0.38 MeV).

Band 2 is intense enough to allow us to extract a mean B(M1)/B(E2) ratio value of 14 ± 4 $(\mu_N/eb)^2$, which is consistent with the suggested configuration. Therefore we propose the following assignments : ABE11 for band 2 and ABF11 for the weaker band 3. As it will be discussed in the next paragraph the two orbitals, $p_{3/2}$ (Ω=3/2) and $f_{5/2}$ (Ω=5/2), are located within about 100 keV. So it is impossible to determine precisely which are E and F orbitals, since they are probably both admixtures of the $p_{3/2}$ and $f_{5/2}$ orbitals even at these low deformations.

Band 1b cannot be understood by analogy with neighbouring odd lead isotopes. Moreover, the spin values of all band heads, which differ by 1 or 2 $\hbar$ from one odd lead isotope to another, are not yet explained. So let us discuss the properties of the bands in ^{193}Pb in the framework of static constrained Hartree-Fock+BCS calculations [27-28], using the Skyrme effective interaction with the parametrization SkM*. This treatment has been already applied to the dipole bands in ^{192}Hg described in reference [32]. In that case, independent multiquasiparticle (1 qp, 3 qp, 5 qp, 7 qp...) excitations with no residual interaction and no Coriolis treatment between the rotational structures were constructed. Figure 7 presents the neutron single particle spectra versus the deformation for oblate shapes for ^{192}Pb. As for all neighbouring lead isotopes the ground state in ^{192}Pb has a spherical shape. But if we now consider the two quasiproton K=11$^-$ excitation, the stabilization of the potential energy is obtained for an oblate deformation with a mass quadrupole moment around Q_{0m}=-12 b, corresponding to a charge quadrupole moment of Q_{0c}=-5.1 eb. Since all the bands observed in the ^{193}Pb nucleus are interpreted as built on the K=11$^-$ excitation, the valence particle states are determined at this oblate deformation. For neutrons near the Fermi level and grouped within less than 2 MeV of each other the following valence orbitals are available (see Figure 7) : Ω^π= 3/2$^-$($p_{3/2}$), 5/2$^-$($f_{5/2}$), 3/2$^+$($i_{13/2}$), 1/2$^+$ ($i_{13/2}$), 1/2$^-$($p_{3/2}$) above and 5/2$^+$($i_{13/2}$), 7/2$^+$($i_{13/2}$), 1/2$^-$($h_{9/2}$), 3/2$^-$($h_{9/2}$), 9/2$^+$($i_{13/2}$) below.

An initial result of our theoretical calculations gives an explanation of the general trend observed for the band-head spins of the lead isotopic series involving the $i_{13/2} \otimes K$=11$^-$ coupling. Indeed if we consider for instance the most intense A11 dipole band, the experimental spins are 25/2$^-$ (^{199}Pb [15]), 27/2$^-$ (^{197}Pb [18]), 27/2$^-$ (^{195}Pb [20]) and 29/2$^-$ (^{193}Pb, this work). When decreasing the mass number from A=200 down to A=192, the Fermi level reaches deeper into the $i_{13/2}$ subshells with larger Ω projections (i.e. less aligned to the rotational axis) such as Ω = 3/2, 5/2 and 7/2 for ^{192}Pb. This phenomenon

appears more clearly by considering the corresponding quasiparticle scheme. One can see in Figure 8 the evolution of the valence quasiparticle energies for the $i_{13/2}$ and $h_{9/2}$ orbitals. The lowest configuration of the $i_{13/2}$ shell is $\Omega = 1/2$ for ^{200}Pb, ^{198}Pb and ^{196}Pb, $\Omega = 3/2$ for ^{194}Pb and $\Omega = 5/2$ for ^{192}Pb, independently of the deformation in a range from $Q_{0m} = -6$ to -12 b. If now we calculate geometrically with the simplest model the total spin value resulting from the coupling of the quasiproton K=11^- configuration along the symmetry axis with an $i_{13/2}$ quasineutron we obtain different values when selecting different Ω projections (Figure 9). By taking the lowest theoretical Ω values, namely Ω=1/2 for ^{200}Pb and Ω=5/2 for ^{192}Pb, the calculations reproduce this evolution, i.e. the increase of the band-head spin when A decreases.

The same shifts of around 1 or 2 $\hbar$ are found for the other bands in ^{193}Pb as ABC11 and ABE/F11 which contain at least one $i_{13/2}$ quasineutron in their configurations.

Concerning now the last band 1b observed at about 600 keV above the band head of band 1a ; one can exclude its interpretation as a seven quasiparticle (like ABC11 + 2 qp) excitation for the two following reasons :

i) Band 1b would be expected at a much higher exitation energy. It appears at relatively similar energy than band 1a. Moreover, band 1b does not decay to band 1a, which would be expected if it was built on ABC11.

ii) The alignment along the rotational axis of bands 1-1b plotted in Figure 5d is similar to that of bands 1-1a. The experimental gain of about 4 $\hbar$ is not enough to be caused by a seven quasiparticle excitation.

We propose two configurations :

• $\nu\left(i_{13/2}\right)^3 \otimes \pi\left([505]9/2^- \otimes [606]13/2^+\right)_{K=11^-}$ by considering larger Ω projections for one or two of the three $i_{13/2}$ subshells than those needed for band 1a. For instance in order to reproduce the experimental spin value of 49/2 $\hbar$ we can couple the three $\Omega = \{1/2, 3/2, 5/2\}$ to $K = 11^-$ with the generalization of the formula used for the A11 coupling :

$$I^2 = \left(11 + \sum_i \Omega_i\right)^2 + \left(\sum_i \sqrt{\left(\frac{13}{2}\right)^2 - \Omega_i^2}\right)^2$$

It is worth noting that in that case we should observe some cross-talk transitions between bands 1a and 1b, their non-observation is probably due to the weak intensity of the bands.

• $\nu\left(\left(i_{13/2}\right) \otimes \left(h_{9/2}\right)^2\right) \otimes \pi\left([505]9/2^- \otimes [606]13/2^+\right)_{K=11^-}$ because of the presence of the $h_{9/2}$ orbital near the Fermi level in ^{192}Pb as shown in Figure 8.

According to our calculations the first configuration energy is closer to the experimental one, but the difference with the second configuration involving two $h_{9/2}$ quasineutrons is not significant enough to distinguish between both proposed assignments.

Another approach, different to the strong coupling model, is the tilted-axis cranking (TAC) model [29] which has been successfully applied in heavier $^{197,199-202}$Pb isotopes [18,15,19]. In this model, both proton and neutron angular momentum components perpendicular to the total angular momentum decrease, implying a gradual alignment ; the so called "shears effect". A direct consequence of the "shears effect" is a decrease of the B(M1) values along the bands. Such experimental B(M1) values have been obtained in $^{196-199}$Pb nuclei [17,21-24] and show a decrease with increasing spin within the bands as expected for the "shears mechanism". For the lightest lead isotopes only B(M1)/B(E2) ratios are available and no significant variations of these values have been observed. In our results in ^{193}Pb, we can just note a slight decrease of this ratio within band 1 when the spin increases but only with three values (see Table 2). Lifetime or more B(M1)/B(E2) ratios are required in order to conclude on the validity of the "shears effect" in the lightest lead isotopes.

IV. Conclusions

Five new dipole $\Delta I = 1$ bands have been identified and connected to the level scheme in ^{193}Pb. A difference of 1-2 $\hbar$ for the band-head spin has been established in the dipole bands at variance with the similar ones in heavier odd lead isotopes. These results have been explained in the framework of microscopic Hartree-Fock+BCS calculations and configurations proposed for the five structures. The prominence of large Ω orbitals of the $\nu\left(i_{13/2}\right)$ shell has been demonstrated. Lifetime measurements will be necessary to assess the validity of the TAC model for the light lead isotopes.

Acknowledgements

We would like to thank all those involved in the setting up and commissioning of EUROGAM 2, especially D. Curien, G. Duchêne and G. de France. We are especially indebted to A. Meens of the CRN Strasbourg for manufacturing the targets and the crew of the VIVITRON. We are grateful to J. Meyer for the theoretical calculations on lead isotopes and D.C. Radford for providing the "Radware" analysis software. The EUROGAM project is funded jointly by IN2P3 (France) and EPSRC (UK). One of us (ANW) acknowledges the receipt of an EPSRC postgraduate studentship.

References

[1] Moore E.F. et al., Phys. Rev. Lett. **63**, 360 (1989)
[2] Hugues J.R. et al., Phys. Rev. C**51** 447 (1995)
[3] Ducroux L. et al., Phys. Rev. C**53** 2701 (1996)
[4] Clark R.M. et al., Phys. Lett. B**275** 247 (1992)
[5] Baldsiefen G. et al., Phys. Lett. B**275** 252 (1992)
[6] Fant B. et al., J. of Phys. G**17** 319 (1991)
[7] Clark R.M. et al., Z. Phys. A**342** 371 (1992)
[8] Baldsiefen G. et al., Z. Phys. A**343** 245 (1992)
[9] Kuhnert A. et al., Phys. Rev. C**46** 133 (1992)
[10] Dagnall P.J. et al., J. of Phys. G**19** 465 (1993)
[11] Hugues J.R. et al., Phys. Rev. C**47** R1337 (1993)
[12] Clark R.M. et al., Nucl. Phys. A**562** 121 (1993)
[13] Plompen A.J.M et al. Nucl. Phys. A**562** 61 (1993)
[14] Porquet M.G. et al., J. of Phys. G**20** 765 (1994)
[15] Baldsiefen G. et al., Nucl. Phys. A**574** 521 (1994)
[16] Fant B. et al., Phys. Scr. T**56** 245 (1995)
[17] Moore E.F. et al., Phys. Rev C**51** 115 (1995)
[18] Baldsiefen G. et al., Nucl. Phys. A**587** 562 (1995)
[19] Baldsiefen G. et al., Nucl. Phys. A**592** 365 (1995)
[20] Kaci M. et al, Z. Phys. A**354** 267 (1996)
[21] Wang T.F. et al., Phys. Rev. Lett. **69** 1737 (1992)
[22] Hugues J.R. et al., Phys. Rev C**48** 2135 (1993)
[23] Clark R.M. et al., Phys. Rev C**50** 84 (1994)
[24] Neffgen M. et al., Nucl. Phys. A**595** 499 (1995)
[25] Lagrange J.M. et al, Nucl. Phys. A**530** 437 (1991)
[26] Nolan P.J., Nucl. Phys. A**520** 657c (1990)
[27] Bonche P. et al., Nucl. Phys. A**519** 509 (1990)
[28] Meyer J. et al., Nucl. Phys. A**588** 597 (1995) and private communication.
[29] Frauendorf S., Nucl. Phys. A**557** 259c (1993)
[30] Radford D., Nucl. Inst. Meth. A**361** 297 (1995)
[31] Hübel H. et al., Nucl. Phys. A**453** 316 (1986)
[32] Le Coz Y. et al., Z. Phys. A**348** 87 (1994)

Table captions

Table 1 Energies, total intensities (corrected for detector efficiency and electron internal conversion) normalized at 100% for the $17/2^+ \rightarrow 13/2^+$ 881.6 keV transition, angular distribution coefficient a_2 and assignments of transitions in ^{193}Pb.

Table 2 B(M1)/B(E2) ratios measured in ^{193}Pb.

Figure captions

Figure 1 Partial level scheme of ^{193}Pb. The energies are indicated in keV and the width of the arrows is proportional to the total intensity of the transitions.

Figure 2 Background-subtracted triple-gated spectra for dipole bands 1, 1a and 1b in ^{193}Pb. The gates are labelled by $*$ and the transition energies of the bands are indicated in keV. For each spectrum, the transitions of the other bands in coincidence are indicated by their corresponding band label and the transitions decaying the band are labelled by their energy and spins.

Figure 3 Background-subtracted triple-gated spectra for dipole bands 2 and 3 in ^{193}Pb. The gates are labelled by $*$ and the transition energies of the bands are indicated in keV and the transitions decaying the band are labelled by their energy and spins.

Figure 4 Experimental excitation energies of band heads for A11, ABC11, ABE/F11 and ABC configurations in ^{193,195,197,199,201}Pb (this work and [20,18,15,19]).

Figure 5 Comparison between the angular momentum along the rotational axis for all the new dipole structures in ^{193}Pb and dipole bands in ^{195}Pb [20], ^{197}Pb [18] and ^{199}Pb [15] as a function of the rotational frequency.

Figure 6 Dynamical moments of inertia for similar bands in ^{193}Pb (band 2) and ^{194}Pb (band c [12]) as a function of the rotational frequency.

Figure 7 Neutron single particle energies as a function of the mass quadrupole moment in ^{192}Pb for oblate shapes obtained by HF+BCS calculations [28] using the SkM* effective force. For each orbital the corresponding Ω value is indicated.

Figure 8 Quasineutron energies of valence $i_{13/2}$ (line) and $h_{9/2}$ (dashed line) subshells for ^{192,194,198,200}Pb, obtained by HF+BCS calculations [28] using the SkM* effective force. For each mass number the deformation has been determined at the two quasiproton $K = 11^-$ stabilization point and the lowest orbital taken as reference for the quasiparticle energies.

Figure 9 Schematic representation of the coupling of a two quasiproton $K = 11^-$ excitations along the deformation axis to an $i_{13/2}$ quasineutron with varying Ω projections.

$E_\gamma(keV)$	I_{tot}	a_2	Assignment
GROUP A			
(40.9)	-	-	$(\frac{25}{2}^+) \rightarrow (\frac{23}{2}^+)$
(66.5)	-	-	$(\frac{21}{2}^-) \rightarrow (\frac{19}{2}^+)$
(72.1)	-	-	$\frac{25}{2}^+ \rightarrow \frac{23}{2}^+$
158.1	18.6 (1.7)	-0.21 ± 0.04	$\frac{29}{2}^- \rightarrow \frac{27}{2}^+$
184.0	13.6 (1.3)	0.12 ± 0.05	$\frac{21}{2}^- \rightarrow \frac{21}{2}^+$
212.9	25.9 (2.2)	-0.18 ± 0.07	$\frac{27}{2}^+ \rightarrow \frac{25}{2}^+$
219.0	8.4 (0.8)	0.19 ± 0.11	$\frac{25}{2}^+ \rightarrow \frac{25}{2}^+$
431.9	3.4 (0.7)	0.28 ± 0.14	$\frac{27}{2}^+ \rightarrow \frac{25}{2}^+$
497.3	1.0 (0.4)	1.13 ± 0.36	$(\frac{19}{2}^+) \rightarrow \frac{15}{2}^+$
520.1	81.9 (3.5)	0.20 ± 0.05	$\frac{21}{2}^+ \rightarrow \frac{17}{2}^+$
527.8	13.8 (1.0)	0.18 ± 0.10	$\frac{19}{2}^+ \rightarrow \frac{15}{2}^+$
591.1	28.3 (1.7)	0.22 ± 0.10	$\frac{23}{2}^+ \rightarrow \frac{19}{2}^+$
593.1	34.6 (2.1)	0.19 ± 0.07	$\frac{25}{2}^+ \rightarrow \frac{21}{2}^+$
622.3	4.4 (0.8)	-	$(\frac{23}{2}^+) \rightarrow \frac{19}{2}^+$
668.2	18.9 (1.3)	-0.46 ± 0.11	$\frac{19}{2}^+ \rightarrow \frac{17}{2}^+$
739.7	23.8 (1.4)	-0.45 ± 0.07	$\frac{23}{2}^+ \rightarrow \frac{21}{2}^+$
811.9	8.0 (0.5)	0.25 ± 0.08	$\frac{25}{2}^+ \rightarrow \frac{21}{2}^+$
881.6	100	0.19 ± 0.05	$\frac{17}{2}^+ \rightarrow \frac{13}{2}^+$
1022.3	14.3 (0.5)	-0.11 ± 0.09	$\frac{15}{2}^+ \rightarrow \frac{13}{2}^+$
GROUP B			
(41.5)	-	-	$(\frac{39}{2}^+) \rightarrow (\frac{37}{2}^+)$
85.6	-	-	$\frac{33}{2}^+ \rightarrow \frac{29}{2}^+$
98.2	5.5 (0.5)	-	$\frac{27}{2}^+ \rightarrow \frac{27}{2}^+$
146.0	6.2 (0.8)	-0.35 ± 0.11	$(\frac{37}{2}^+) \rightarrow (\frac{35}{2}^+)$
148.4	9.7 (1.6)	-0.42 ± 0.14	$(\frac{39}{2}^+) \rightarrow (\frac{37}{2}^+)$
164.0	7.4 (0.8)	-0.41 ± 0.10	$(\frac{35}{2}^+) \rightarrow \frac{33}{2}^+$
196.9	3.5 (0.8)	-0.19 ± 0.15	$(\frac{41}{2}^+) \rightarrow (\frac{39}{2}^+)$
234.5	1.1 (0.3)	-	$(\frac{39}{2}^+) \rightarrow (\frac{37}{2}^+)$
279.2	5.4 (0.6)	-0.19 ± 0.10	$(\frac{41}{2}^+) \rightarrow (\frac{39}{2}^+)$
294.8	0.2 (0.1)	0.13 ± 0.19	$(\frac{37}{2}^+) \rightarrow (\frac{33}{2}^+)$
296.3	7.9 (0.5)	-0.40 ± 0.09	$\frac{31}{2}^+ \rightarrow \frac{29}{2}^+$
296.4	0.6 (0.3)	-	$(\frac{39}{2}^+) \rightarrow (\frac{37}{2}^+)$
311.1	16.3 (1.0)	-0.32 ± 0.10	$\frac{27}{2}^+ \rightarrow \frac{25}{2}^+$
324.0	0.2 (0.1)	-	$(\frac{37}{2}^+) \rightarrow (\frac{33}{2}^+)$
338.7	0.5 (0.2)	-	$(\frac{41}{2}^+) \rightarrow (\frac{39}{2}^+)$
342.7	10.5 (0.6)	-0.28 ± 0.05	$\frac{29}{2}^+ \rightarrow \frac{27}{2}^+$
364.0	7.8 (0.5)	-0.36 ± 0.11	$\frac{31}{2}^+ \rightarrow \frac{29}{2}^+$
367.9	4.3 (0.6)	-0.19 ± 0.08	$(\frac{43}{2}^+) \rightarrow (\frac{41}{2}^+)$
377.3	0.6 (0.3)	-	$(\frac{37}{2}^+) \rightarrow \frac{35}{2}^+$
382.0	2.4 (0.4)	-0.18 ± 0.12	$\frac{35}{2}^+ \rightarrow \frac{33}{2}^+$
388.7	1.2 (0.5)	-	$\frac{37}{2}^+ \rightarrow \frac{35}{2}^+$
395.8	5.6 (0.6)	0.21 ± 0.06	$\frac{35}{2}^+ \rightarrow \frac{31}{2}^+$
409.5	4.7 (0.4)	-0.46 ± 0.08	$\frac{33}{2}^+ \rightarrow \frac{31}{2}^+$
419.6	1.5 (0.4)	0.23 ± 0.10	$(\frac{39}{2}^+) \rightarrow \frac{35}{2}^+$
438.7	1.7 (0.4)	-0.27 ± 0.10	$(\frac{37}{2}^+) \rightarrow (\frac{35}{2}^+)$
448.1	1.5 (0.4)	-	$(\frac{39}{2}^+) \rightarrow \frac{37}{2}^+$
448.9	0.6 (0.3)	-	$(\frac{35}{2}^+) \rightarrow \frac{33}{2}^+$

$E_\gamma(keV)$	I_{tot}	a_2	Assignment
461.2	0.5 (0.2)	-	$(\frac{35}{2}^+) \rightarrow \frac{33}{2}^+$
461.5	0.7 (0.3)	-	$\frac{31}{2}^+ \rightarrow \frac{29}{2}^+$
462.9	14.3 (1.1)	-0.35 ± 0.10	$\frac{33}{2}^+ \rightarrow \frac{31}{2}^+$
510.2	0.5 (0.2)	-	$\frac{35}{2}^+ \rightarrow \frac{33}{2}^+$
532.4	3.5 (0.5)	0.10 ± 0.08	$\frac{29}{2}^+ \rightarrow \frac{25}{2}^+$
540.4	0.2 (0.2)	-	$(\frac{35}{2}^+) \rightarrow \frac{33}{2}^+$
545.3	0.2 (0.1)	-	$(\frac{39}{2}^+) \rightarrow \frac{37}{2}^+$
555.4	12.2 (1.0)	-0.43 ± 0.08	$\frac{29}{2}^+ \rightarrow \frac{27}{2}^+$
567.5	1.2 (0.4)	-	$(\frac{39}{2}^+) \rightarrow (\frac{37}{2}^+)$
581.8	1.1 (0.4)	0.15 ± 0.14	$(\frac{37}{2}^+) \rightarrow \frac{33}{2}^+$
609.9	1.2 (0.3)	0.50 ± 0.14	$(\frac{33}{2}^+) \rightarrow \frac{29}{2}^+$
644.1	0.4 (0.2)	0.39 ± 0.23	$(\frac{41}{2}^+) \rightarrow \frac{37}{2}^+$
677.6	12.5 (1.2)	0.19 ± 0.08	$\frac{29}{2}^+ \rightarrow \frac{25}{2}^+$
701.7	1.7 (0.3)	0.24 ± 0.12	$\frac{37}{2}^+ \rightarrow \frac{33}{2}^+$
706.7	1.6 (0.2)	0.40 ± 0.23	$\frac{31}{2}^+ \rightarrow \frac{27}{2}^+$
742.3	5.3 (0.8)	0.22 ± 0.08	$\frac{33}{2}^+ \rightarrow \frac{29}{2}^+$
755.1	1.0 (0.2)	0.37 ± 0.21	$(\frac{33}{2}^+) \rightarrow \frac{29}{2}^+$
759.4	2.6 (0.3)	0.25 ± 0.11	$\frac{33}{2}^+ \rightarrow \frac{29}{2}^+$
770.2	0.4 (0.2)	-	$\frac{37}{2}^+ \rightarrow \frac{33}{2}^+$
773.5	0.7 (0.3)	-	$\frac{33}{2}^+ \rightarrow \frac{29}{2}^+$
791.5	0.8 (0.2)	0.84 ± 0.31	$\frac{35}{2}^+ \rightarrow \frac{31}{2}^+$
851.7	15.4 (1.2)	0.17 ± 0.09	$\frac{31}{2}^+ \rightarrow \frac{27}{2}^+$
946.0	0.1 (0.1)	-	$(\frac{37}{2}^+) \rightarrow \frac{33}{2}^+$
1030.1	0.1 (0.1)	-	$(\frac{33}{2}^+) \rightarrow \frac{29}{2}^+$
1145.2	0.3 (0.1)	0.38 ± 0.33	$(\frac{33}{2}^+) \rightarrow \frac{29}{2}^+$
1174.9	0.2 (0.1)	-	$(\frac{33}{2}^+) \rightarrow \frac{29}{2}^+$
GROUP C			
180.0	5.7 (0.4)	-0.12 ± 0.06	$\frac{27}{2}^- \rightarrow \frac{25}{2}^-$
204.6	0.3 (0.1)	-	$\frac{29}{2}^+ \rightarrow \frac{27}{2}^-$
263.1	0.7 (0.2)	-	$\frac{27}{2}^- \rightarrow \frac{23}{2}^-$
341.0	0.6 (0.2)	0.13 ± 0.19	$\frac{31}{2}^- \rightarrow \frac{27}{2}^-$
385.0	0.6 (0.3)	-	$\frac{29}{2}^- \rightarrow \frac{27}{2}^-$
421.4	0.5 (0.2)	-	$\frac{31}{2}^- \rightarrow \frac{29}{2}^-$
472.7	1.3 (0.5)	-0.30 ± 0.13	$\frac{23}{2}^- \rightarrow \frac{21}{2}^-$
547.0	1.3 (0.4)	0.26 ± 0.12	$(\frac{35}{2}^-) \rightarrow \frac{31}{2}^-$
542.7	0.4 (0.2)	0.01 ± 0.19	$(\frac{31}{2}^-) \rightarrow \frac{29}{2}^-$
556.0	6.1 (0.5)	0.30 ± 0.05	$\frac{25}{2}^- \rightarrow \frac{21}{2}^-$
565.0	1.3 (0.3)	0.26 ± 0.12	$\frac{29}{2}^- \rightarrow \frac{25}{2}^-$
595.0	0.7 (0.4)	-	$\frac{27}{2}^- \rightarrow (\frac{23}{2}^-)$
613.2	1.7 (0.5)	0.30 ± 0.11	$(\frac{35}{2}^-) \rightarrow \frac{31}{2}^-$
638.7	0.8 (0.3)	0.21 ± 0.13	$(\frac{39}{2}^-) \rightarrow (\frac{35}{2}^-)$
657.4	0.4 (0.2)	0.21 ± 0.25	$(\frac{39}{2}^-) \rightarrow (\frac{35}{2}^-)$
672.6	1.2 (0.4)	0.19 ± 0.12	$\frac{31}{2}^- \rightarrow \frac{27}{2}^-$
693.4	0.5 (0.2)	0.39 ± 0.22	$(\frac{39}{2}^-) \rightarrow (\frac{35}{2}^-)$
712.8	0.4 (0.2)	0.83 ± 0.33	$(\frac{43}{2}^-) \rightarrow (\frac{39}{2}^-)$
730.6	0.4 (0.2)	-	$(\frac{43}{2}^-) \rightarrow (\frac{39}{2}^-)$
766.6	0.2 (0.1)	-	$(\frac{43}{2}^-) \rightarrow (\frac{39}{2}^-)$
806.4	2.0 (0.4)	0.37 ± 0.18	$\frac{31}{2}^- \rightarrow \frac{27}{2}^-$

$E_\gamma(keV)$	I_{tot}	a_2	Assignment
GROUP D			
156.5	0.7 (0.3)	-	$(\frac{37}{2}^-) \rightarrow (\frac{35}{2}^-)$
158.0	0.6 (0.3)	-	$(\frac{33}{2}^-) \rightarrow (\frac{31}{2}^-)$
175.9	0.2 (0.2)	-0.32 ± 0.15	$(\frac{45}{2}^-) \rightarrow (\frac{43}{2}^-)$
208.0	1.2 (0.3)	-0.06 ± 0.12	$(\frac{39}{2}^-) \rightarrow (\frac{37}{2}^-)$
231.1	1.0 (0.4)	-0.22 ± 0.15	$(\frac{45}{2}^-) \rightarrow (\frac{43}{2}^-)$
261.7	0.8 (0.3)	-0.32 ± 0.11	$(\frac{41}{2}^-) \rightarrow (\frac{39}{2}^-)$
264.8	0.3 (0.2)	-	$(\frac{45}{2}^-) \rightarrow (\frac{43}{2}^-)$
295.2	0.3 (0.2)	-0.17 ± 0.16	$(\frac{43}{2}^-) \rightarrow (\frac{41}{2}^-)$
303.4	0.8 (0.3)	-0.39 ± 0.11	$\frac{41}{2}^- \rightarrow \frac{39}{2}^-$
319.6	1.6 (0.4)	-0.39 ± 0.10	$(\frac{37}{2}^-) \rightarrow \frac{35}{2}^-$
319.7	0.7 (0.3)	-0.27 ± 0.10	$(\frac{47}{2}^-) \rightarrow \frac{45}{2}^-$
323.6	0.9 (0.3)	-0.34 ± 0.11	$(\frac{49}{2}^-) \rightarrow (\frac{47}{2}^-)$
325.7	0.3 (0.2)	-	$(\frac{43}{2}^-) \rightarrow \frac{41}{2}^-$
328.8	0.4 (0.2)	-	$(\frac{43}{2}^-) \rightarrow (\frac{41}{2}^-)$
353.7	1.2 (0.3)	-0.31 ± 0.09	$(\frac{45}{2}^-) \rightarrow \frac{43}{2}^-$
362.4	0.2 (0.2)	-	$(\frac{47}{2}^-) \rightarrow (\frac{45}{2}^-)$
390.8	0.4 (0.3)	-0.34 ± 0.21	$(\frac{43}{2}^-) \rightarrow \frac{41}{2}^-$
396.6	0.4 (0.3)	-	$(\frac{41}{2}^-) \rightarrow \frac{39}{2}^-$
406.5	0.5 (0.3)	-0.18 ± 0.26	$(\frac{45}{2}^-) \rightarrow (\frac{43}{2}^-)$
415.6	1.3 (0.3)	-0.08 ± 0.15	$(\frac{39}{2}^-) \rightarrow (\frac{37}{2}^-)$
424.1	1.1 (0.2)	-0.20 ± 0.13	$\frac{41}{2}^- \rightarrow \frac{39}{2}^-$
442.0	0.4 (0.3)	-0.49 ± 0.19	$(\frac{43}{2}^-) \rightarrow (\frac{41}{2}^-)$
444.9	2.5 (0.4)	-0.23 ± 0.08	$\frac{39}{2}^- \rightarrow \frac{37}{2}^-$
455.3	0.6 (0.3)	-	$\frac{41}{2}^- \rightarrow \frac{39}{2}^-$
482.9	1.0 (0.2)	-0.21 ± 0.11	$(\frac{41}{2}^-) \rightarrow (\frac{39}{2}^-)$
487.8	0.6 (0.3)	-0.18 ± 0.11	$(\frac{35}{2}^-) \rightarrow (\frac{33}{2}^-)$
675.8	1.0 (0.3)	-	$(\frac{31}{2}^-) \rightarrow \frac{29}{2}^-$
711.7	0.1 (0.1)	-	$(\frac{45}{2}^-) \rightarrow (\frac{41}{2}^-)$
834.0	1.3 (0.4)	0.56 ± 0.14	$(\frac{33}{2}^-) \rightarrow \frac{29}{2}^-$
846.5	0.2 (0.1)	-	$\frac{39}{2}^- \rightarrow \frac{35}{2}^-$
869.1	0.1 (0.1)	-	$\frac{41}{2}^- \rightarrow \frac{37}{2}^-$
1129.5	0.2 (0.1)	-	$(\frac{45}{2}^-) \rightarrow (\frac{41}{2}^-)$
1225.2	0.2 (0.1)	-	$(\frac{43}{2}^-) \rightarrow (\frac{39}{2}^-)$
Band 1			
102.1	16.5 (1.5)	-0.35 ± 0.13	$\frac{31}{2}^- \rightarrow \frac{29}{2}^-$
252.3	17.2 (1.1)	-0.32 ± 0.05	$\frac{33}{2}^- \rightarrow \frac{31}{2}^-$
334.5	2.8 (0.2)	-0.33 ± 0.13	$\frac{41}{2}^- \rightarrow \frac{39}{2}^-$
357.7	1.8 (0.4)	-0.57 ± 0.16	$\frac{43}{2}^- \rightarrow \frac{41}{2}^-$
381.5	13.0 (0.5)	-0.36 ± 0.05	$\frac{35}{2}^- \rightarrow \frac{33}{2}^-$
390.3	1.3 (0.3)	-0.29 ± 0.13	$\frac{45}{2}^- \rightarrow \frac{43}{2}^-$
401.6	7.7 (0.4)	-0.37 ± 0.07	$\frac{37}{2}^- \rightarrow \frac{35}{2}^-$
413.8	4.0 (0.3)	-0.39 ± 0.14	$\frac{39}{2}^- \rightarrow \frac{37}{2}^-$
633.8	0.5 (0.2)	-	$\frac{35}{2}^- \rightarrow \frac{31}{2}^-$
692.3	0.1 (0.1)	-	$(\frac{43}{2}^-) \rightarrow (\frac{39}{2}^-)$
748.3	0.4 (0.2)	-	$\frac{41}{2}^- \rightarrow \frac{37}{2}^-$
783.1	1.0 (0.2)	0.20 ± 0.19	$\frac{37}{2}^- \rightarrow \frac{33}{2}^-$
815.4	0.8 (0.2)	-	$\frac{39}{2}^- \rightarrow \frac{35}{2}^-$

$E_\gamma(keV)$	I_{tot}	a_2	Assignment
Band 1a			
239.1	0.6 (0.3)	-0.20 ± 0.14	$(\frac{47}{2}^-) \rightarrow (\frac{45}{2}^-)$
265.6	0.5 (0.2)	-0.30 ± 0.16	$(\frac{49}{2}^-) \rightarrow (\frac{47}{2}^-)$
329.5	0.5 (0.3)	-0.53 ± 0.13	$(\frac{51}{2}^-) \rightarrow (\frac{49}{2}^-)$
375.6	0.4 (0.3)	-0.59 ± 0.15	$(\frac{53}{2}^-) \rightarrow (\frac{51}{2}^-)$
412.9	0.3 (0.1)	-	$(\frac{55}{2}^-) \rightarrow (\frac{53}{2}^-)$
439.2	0.2 (0.1)	-0.20 ± 0.26	$(\frac{57}{2}^-) \rightarrow (\frac{55}{2}^-)$
Band 1b			
176.3	0.6 (0.2)	-0.47 ± 0.09	$(\frac{51}{2}^-) \rightarrow (\frac{49}{2}^-)$
283.7	0.5 (0.2)	-0.39 ± 0.09	$(\frac{53}{2}^-) \rightarrow (\frac{51}{2}^-)$
311.9	0.4 (0.3)	-0.38 ± 0.14	$(\frac{55}{2}^-) \rightarrow (\frac{53}{2}^-)$
330.4	0.4 (0.2)	-0.44 ± 0.10	$(\frac{57}{2}^-) \rightarrow (\frac{55}{2}^-)$
384.5	0.3 (0.2)	-0.21 ± 0.19	$(\frac{59}{2}^-) \rightarrow (\frac{57}{2}^-)$
401.5	0.2 (0.1)	-	$(\frac{61}{2}^-) \rightarrow (\frac{59}{2}^-)$
Band 2			
90.0	-	-	$(\frac{41}{2}^+) \rightarrow (\frac{39}{2}^+)$
148.9	6.6 (1.0)	-0.62 ± 0.19	$(\frac{43}{2}^+) \rightarrow (\frac{41}{2}^+)$
232.0	6.9 (1.0)	-0.34 ± 0.09	$(\frac{45}{2}^+) \rightarrow (\frac{43}{2}^+)$
291.6	7.0 (0.7)	-0.33 ± 0.05	$(\frac{47}{2}^+) \rightarrow (\frac{45}{2}^+)$
365.2	5.7 (0.5)	-0.38 ± 0.05	$(\frac{49}{2}^+) \rightarrow (\frac{47}{2}^+)$
389.6	4.1 (0.4)	-0.29 ± 0.07	$(\frac{51}{2}^+) \rightarrow (\frac{49}{2}^+)$
416.1	3.2 (0.4)	-	$(\frac{53}{2}^+) \rightarrow (\frac{51}{2}^+)$
426.1	1.2 (0.2)	-	$(\frac{55}{2}^+) \rightarrow (\frac{53}{2}^+)$
432.7	0.6 (0.2)	-	$(\frac{57}{2}^+) \rightarrow (\frac{55}{2}^+)$
(426.1)	0.4 (0.3)	-	$(\frac{59}{2}^+) \rightarrow (\frac{57}{2}^+)$
(416.1)	0.2 (0.2)	-	$(\frac{61}{2}^+) \rightarrow (\frac{59}{2}^+)$
656.8	0.6 (0.2)	-	$(\frac{49}{2}^+) \rightarrow (\frac{45}{2}^+)$
754.7	0.8 (0.2)	-	$(\frac{51}{2}^+) \rightarrow (\frac{47}{2}^+)$
805.6	0.2 (0.1)	-	$(\frac{53}{2}^+) \rightarrow (\frac{49}{2}^+)$
842.2	0.3 (0.1)	-	$(\frac{55}{2}^+) \rightarrow (\frac{51}{2}^+)$
858.8	0.1 (0.1)	-	$(\frac{57}{2}^+) \rightarrow (\frac{53}{2}^+)$
Band 3			
224.3	2.5 (0.4)	-0.57 ± 0.10	$(\frac{45}{2}^+) \rightarrow (\frac{43}{2}^+)$
267.5	2.8 (0.3)	-0.24 ± 0.12	$(\frac{47}{2}^+) \rightarrow (\frac{45}{2}^+)$
326.2	2.2 (0.2)	-0.34 ± 0.10	$(\frac{49}{2}^+) \rightarrow (\frac{47}{2}^+)$
382.4	1.4 (0.3)	-0.43 ± 0.08	$(\frac{51}{2}^+) \rightarrow (\frac{49}{2}^+)$

	E_γ (M1) keV	E_γ (E2) keV	B(M1)/B(E2) ratio $(\mu_N/eb)^2$
Band 1	382 402 414	634 783 815	28 ± 5 22 ± 4 16 ± 6
Band 2	365 390 426	657 755 842	15 ± 3 12 ± 3 15 ± 3

Table 2 Ducroux et al., Z. Phys. A

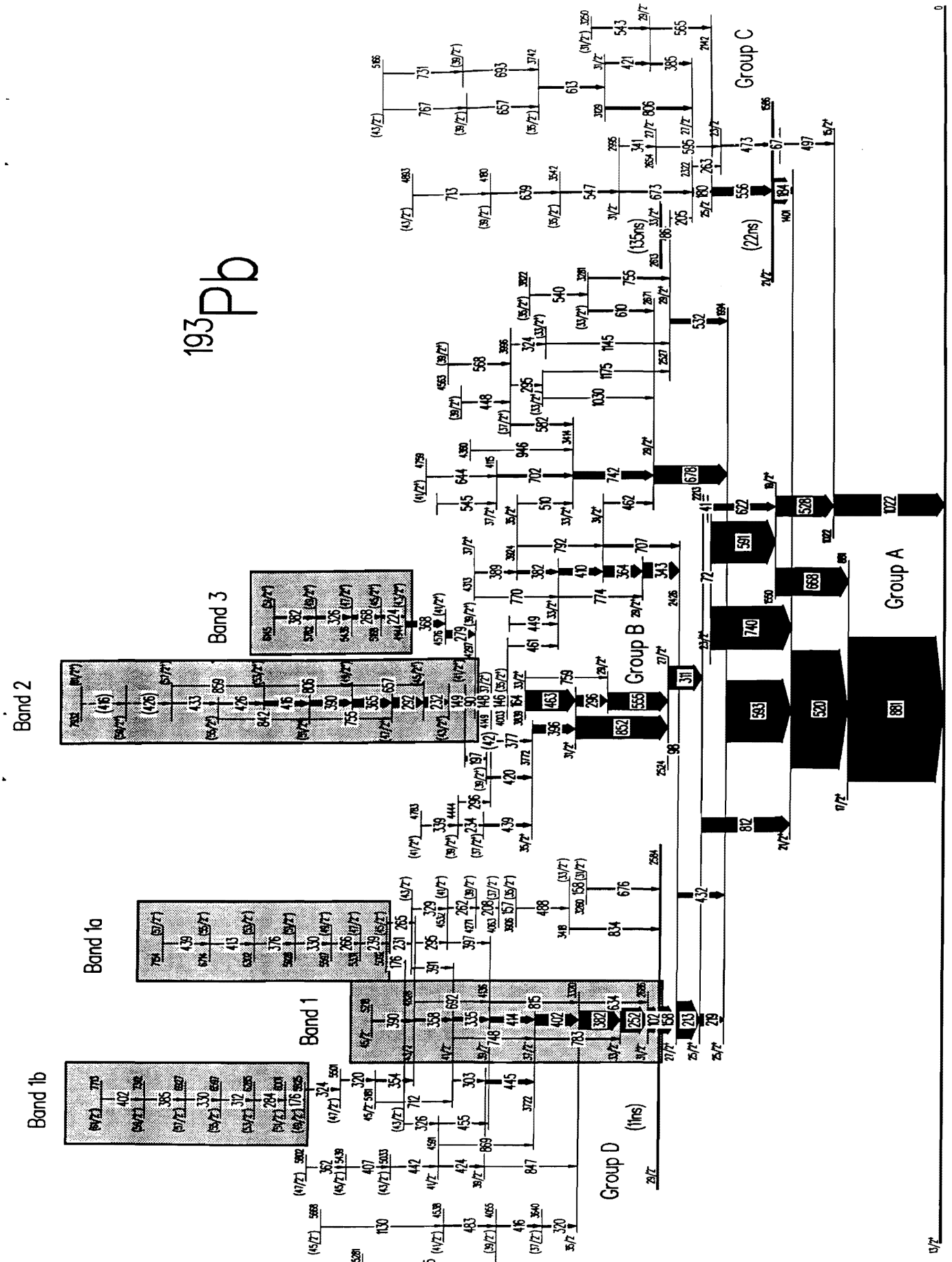

Figure 1 Ducroux et al., Z. Phys. A

Figure 2 Ducroux et al., Z. Phys. A

Figure 3 Ducroux et al., Z. Phys. A

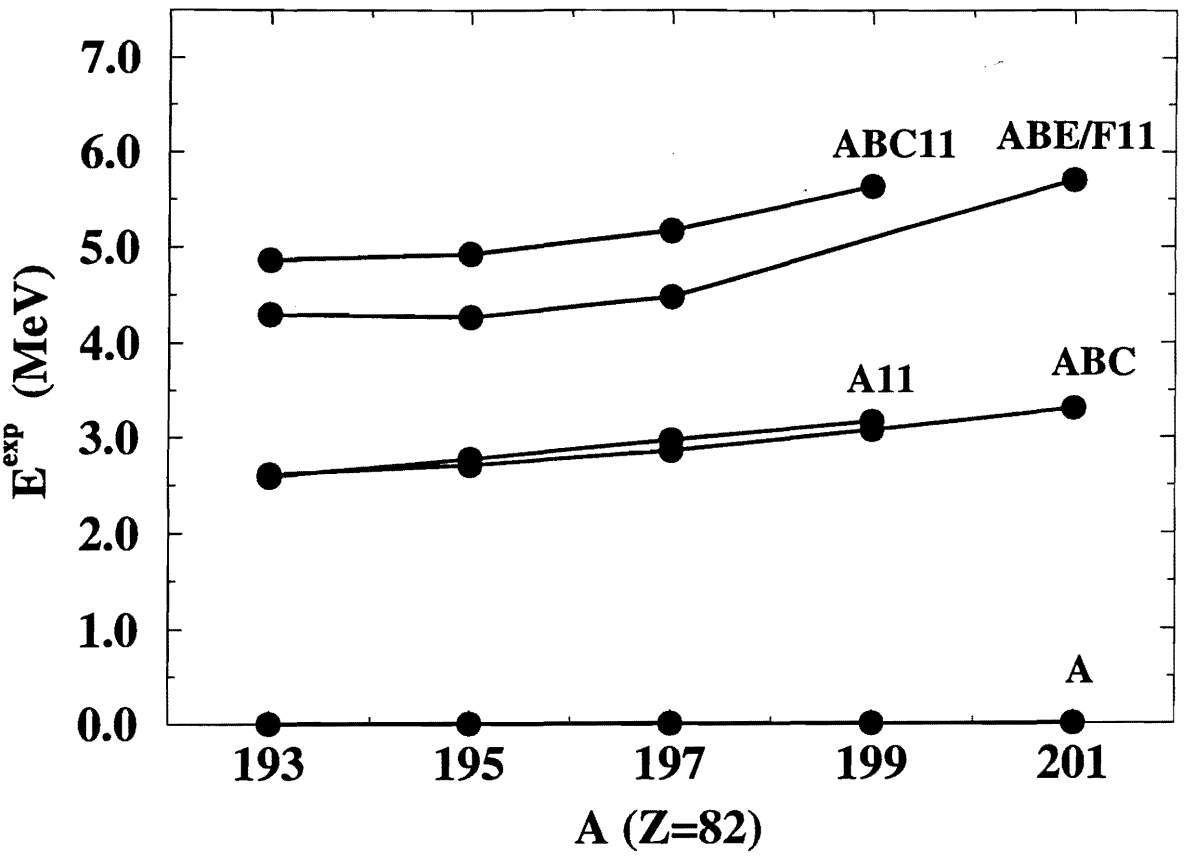

Figure 4 Ducroux et al., Z. Phys. A

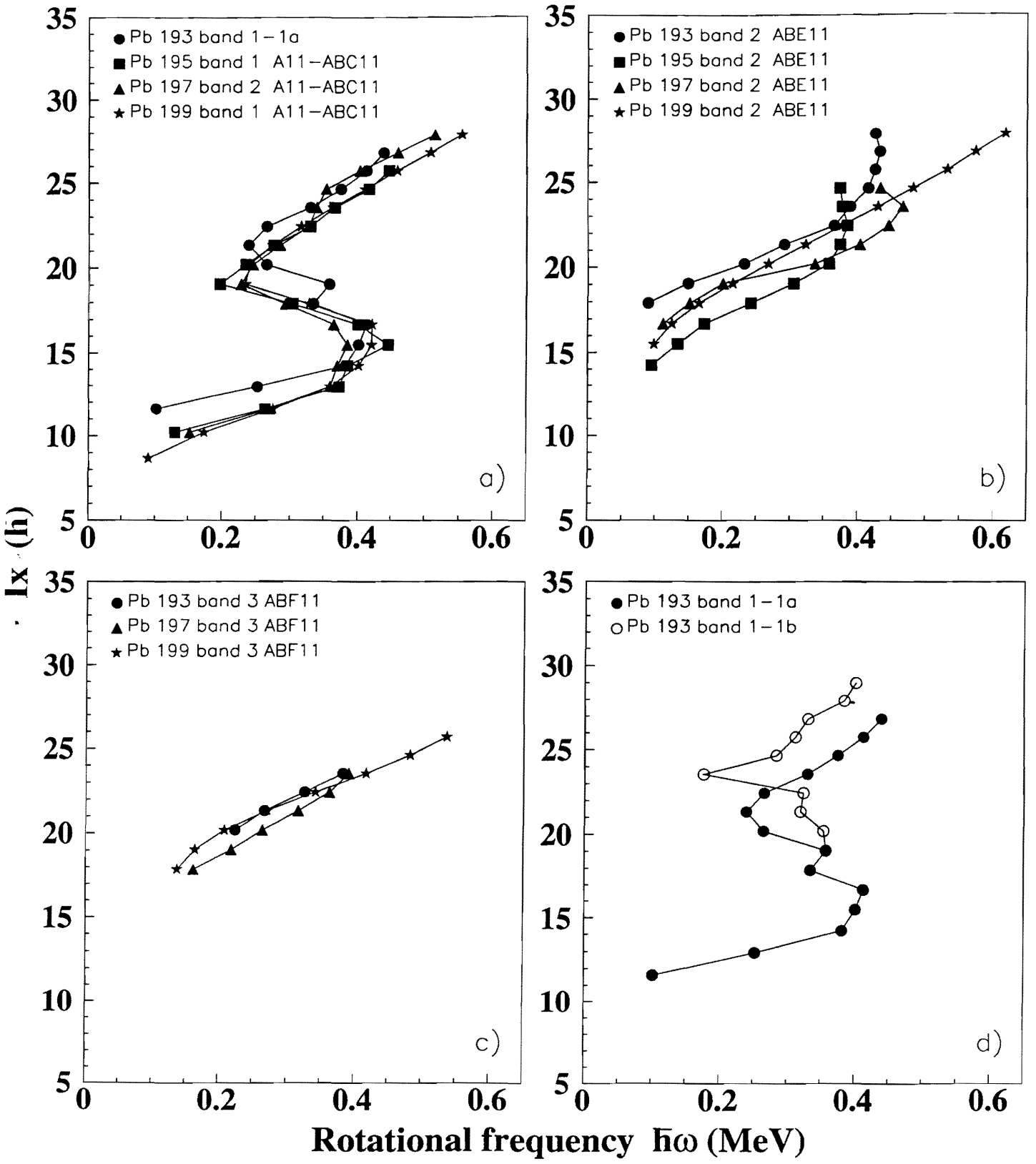

Figure 5 Ducroux et al., Z. Phys. A

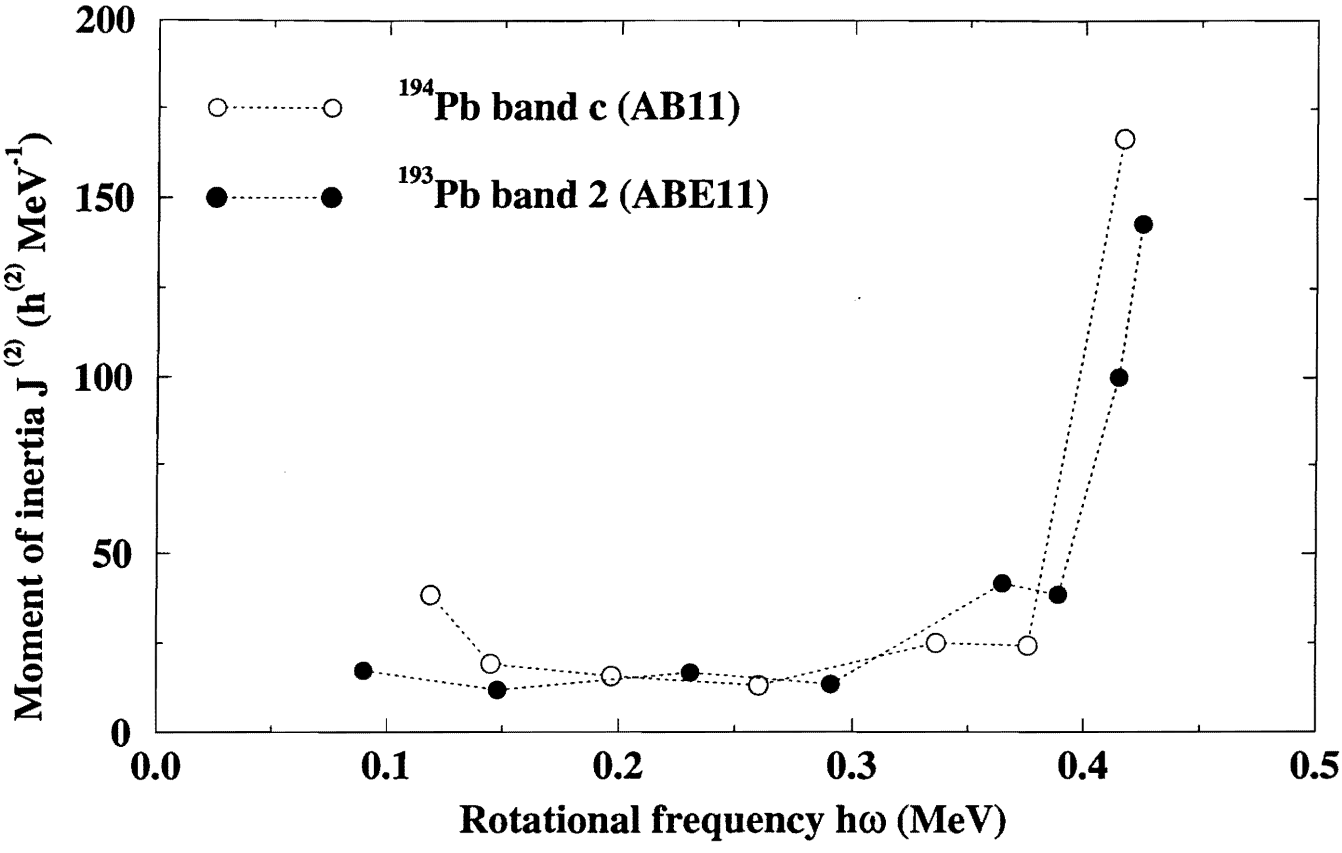

Figure 6 Ducroux et al., Z. Phys. A

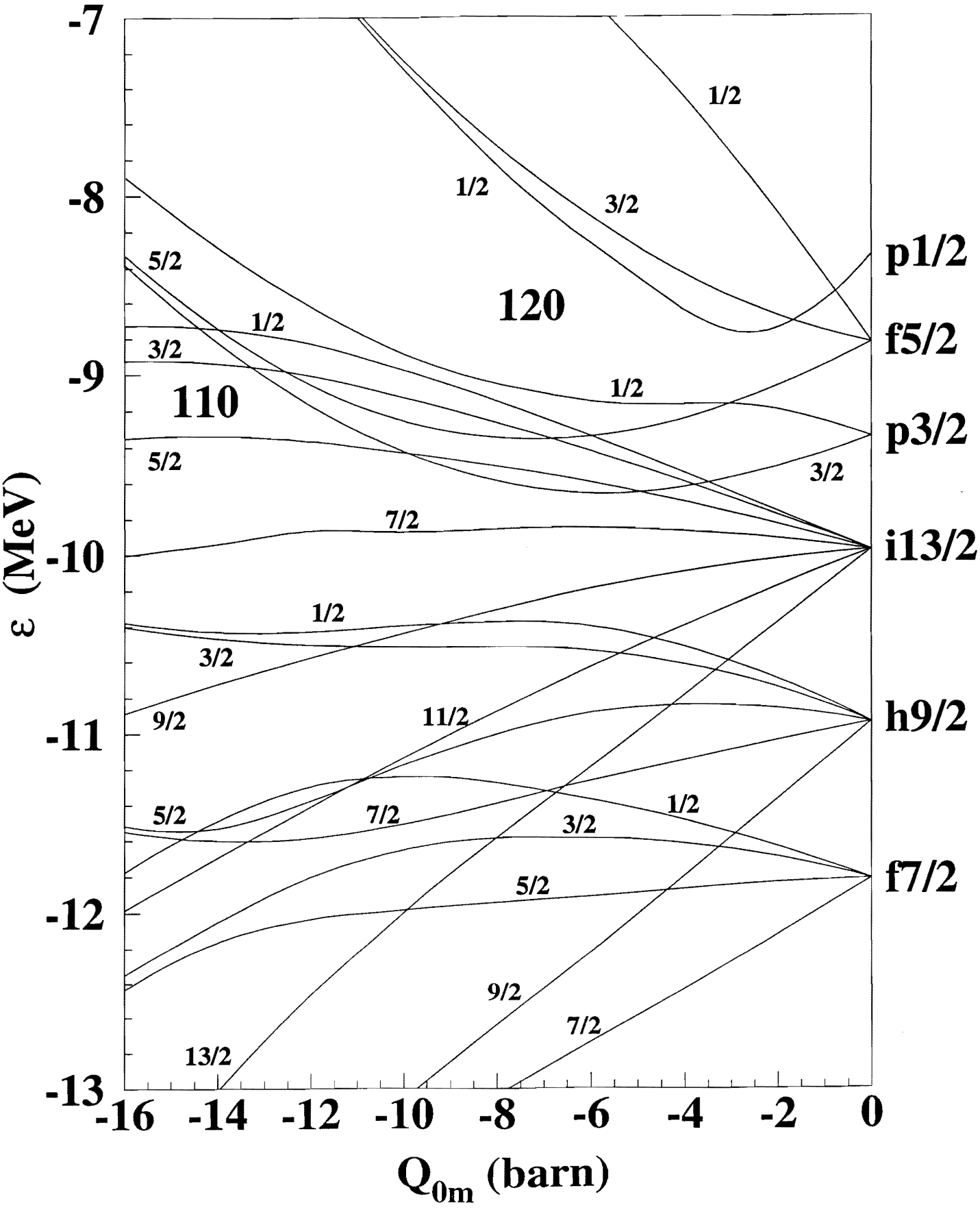

Figure 7 Ducroux et al., Z. Phys. A

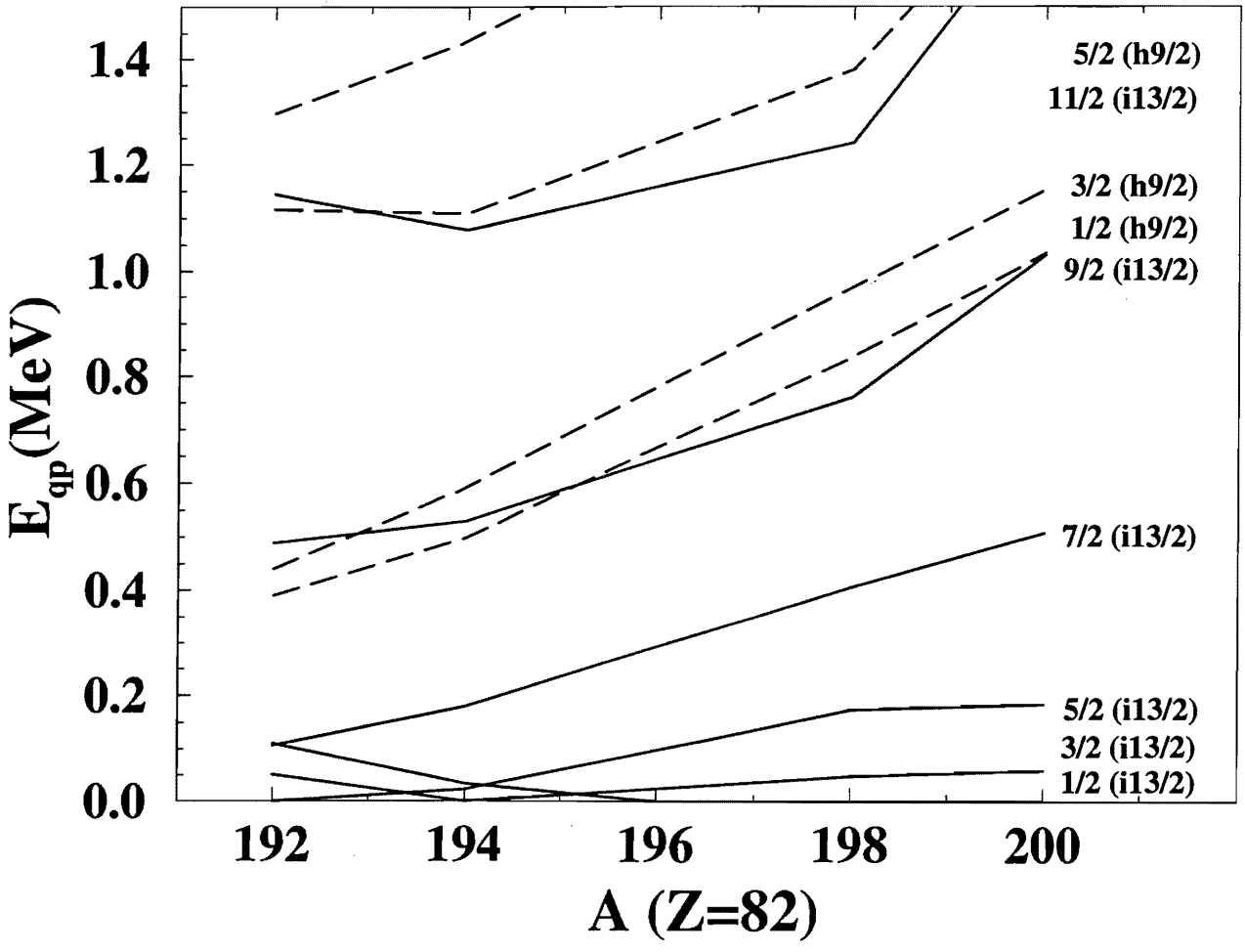

Figure 8 Ducroux et al., Z. Phys. A

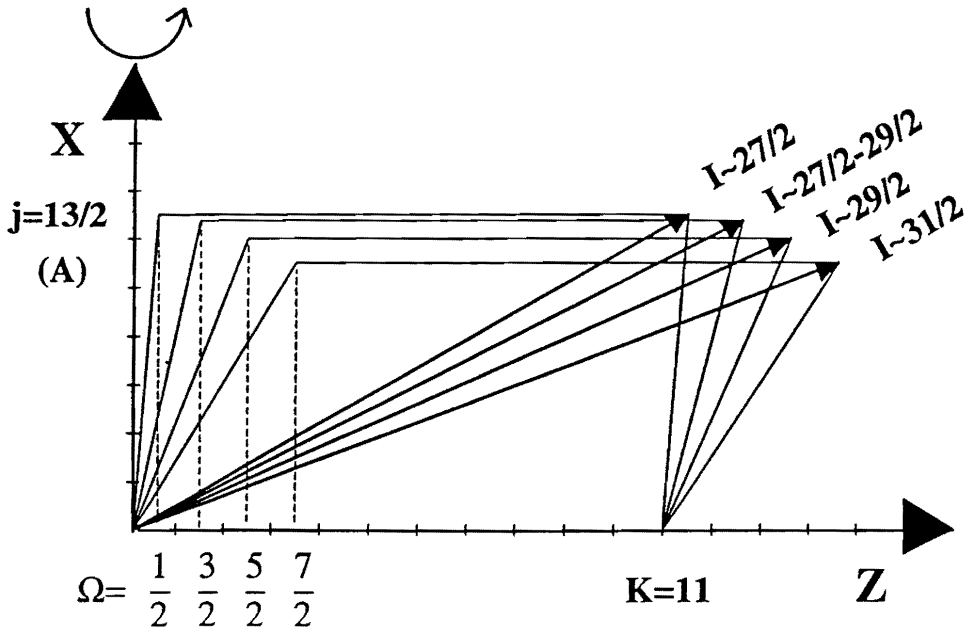

Figure 9 Ducroux et al., Z. Phys. A